Network Percolation and Robustness in LEO Satellite Constellations

An Empirical Analysis of the Masking Effect: Phase Transitions, Structural Vulnerabilities, and Design Parameter Analysis

Mahesh Ramani

Independent

February 2026

Table of Contents

Abstract

This study investigates the connectivity and robustness profiles of Low Earth Orbit (LEO) satellite constellations through the lens of percolation theory. Using a simulation framework developed for this research, an analysis is conducted on how the structured Walker Delta configuration contrasts with randomized Stochastic distributions across multiple design parameters. The empirical analysis demonstrates a masking effect where network redundancy conceals structural vulnerabilities to targeted attacks until a critical failure threshold is reached. Through parameter sweeps of altitude (300–1100 kilometers), inter-satellite link distance (500–3000 kilometers), maximum degree constraints (2–5), constellation density (1000–8000 satellites), phasing (0–100), plane count (10–130), and orbital inclination (30°–90°), design trade-offs are identified and relationships between parameters and network metrics are quantified. Key findings include maximum degree as the dominant robustness factor (correlation coefficient of 0.99 with plane attack resilience), a negative correlation between plane count and attack resilience (correlation coefficient of −0.91), and inclination-dependent robustness patterns with peak performance in the 50°–60° range. The masking threshold varies with maximum degree, ranging from approximately 15% at degree = 2 to 25% at degree = 5. These results provide empirical guidance for constellation design, though limitations including discrete-time snapshot methodology and coarse parameter sampling should be considered.

1. Introduction

The study of network connectivity under random and targeted failures has deep roots in percolation theory, a mathematical framework originally developed to describe the flow of fluids through porous materials. In the context of communication networks, percolation theory provides tools for understanding how connectivity emerges as nodes are added to a system and how it degrades as nodes are removed. The Giant Component Fraction, which represents the proportion of nodes belonging to the largest connected cluster, serves as the order parameter for this phase transition.

Low Earth Orbit satellite constellations present an application domain for percolation theory. These networks, exemplified by operational systems like Starlink and OneWeb, consist of hundreds to thousands of satellites arranged in orbital planes, forming a graph where edges represent inter-satellite links. The geometric regularity of the Walker Delta configuration, a symmetric

arrangement where satellites are distributed evenly across orbital planes, creates structured connectivity patterns that differ from random graphs.

This investigation was motivated by an empirical observation that emerged across simulations conducted: when satellites are removed randomly, the network degrades gradually, but when entire orbital planes are removed (simulating targeted attacks or debris events affecting specific inclinations), the degradation follows a different trajectory. Initially, the two curves are nearly indistinguishable, a phenomenon consistent with the masking effect described in percolation theory, but beyond a threshold, the plane attack curve drops more rapidly while the random failure curve maintains higher connectivity.

In percolation theory, the susceptibility, defined as the sum of squared sizes of finite clusters, peaks at the critical threshold where the giant component first emerges. In satellite networks, the masking zone corresponds to a regime where redundant paths abound, making the network appear robust regardless of attack type. The exit from this zone marks a transition where the geometric structure of the Walker Delta becomes a dominant factor in determining connectivity.

The objectives of this research are to characterize the percolation phase transition in LEO constellations, quantify the masking effect across a parameter space, and identify empirical relationships between design parameters and network performance metrics. To achieve these objectives, a simulation framework was developed that models constellation geometry, constructs network topologies under physical constraints, and computes graph metrics including Giant Component Fraction, algebraic connectivity, clustering coefficient, and average path length.

2. Methodology

2.1 Simulation Framework

A discrete snapshot simulation environment was developed in Python to analyze the connectivity and robustness of LEO constellations. The simulation uses NumPy for vectorized coordinate transformations and SciPy for spatial queries using cKDTree structures and sparse matrix graph operations. To ensure computational efficiency during large-scale topology generation, parallel processing was implemented with multiprocessing pools employing up to ten worker processes.

The simulation implements two computational procedures. The Phase Transition Analysis procedure incrementally increases satellite population from 50 to 5000 in steps of 150 satellites. At each step, the Walker Delta constellation is generated, the adjacency matrix is constructed under physical constraints, and network metrics are computed. This procedure identifies the percolation threshold, which is the density where a Giant Component spans the majority of the network. The

Kessler Syndrome Analysis procedure starts with a fully formed 5000-satellite network and removes nodes to simulate two failure modes: random failure where nodes are removed with uniform probability, and plane attack where entire orbital planes are removed. The masking effect is quantified as the difference between Giant Component Fraction under random failure and plane attack over the fraction removed, with each configuration replicated twelve times using different random seeds to enable statistical confidence interval estimation at the 95% confidence level.

2.2 Constellation Generation

Two constellation models were generated to isolate the effects of geometric structure versus node density. The primary model uses the Walker Delta pattern, distributing satellites as evenly as possible across orbital planes. The position of satellite k in plane j at time t is calculated using orbital elements propagated via mean anomaly. The position vector is derived by applying rotation matrices for inclination and the plane's Right Ascension of the Ascending Node:

$$\mathbf{r}_{jk} = R_z(\Omega_j)\, R_x(i) \begin{pmatrix} a\cos(M_t) \\ a\sin(M_t) \\ 0 \end{pmatrix} \tag{1}$$

where a represents the orbital radius calculated as the sum of Earth's radius and orbital altitude, and the mean motion n is computed as $n = \sqrt{\mu/(a^3)}$ where μ is Earth's gravitational parameter. The phasing parameter determines the relative angular offset between satellites in adjacent planes.

To serve as a control group, a Stochastic model was implemented using uniform spherical distribution via Marsaglia's method. This approach generates satellites with uniform distribution across the spherical shell at the specified altitude, ensuring that performance differences can be attributed to geometric structure rather than node density or altitude.

2.3 Network Topology Construction

For each simulation run, the constellation topology was modeled as an undirected graph $G = (V, E)$ where V represents satellites and E represents inter-satellite links. A strict adjacency algorithm was implemented that constructs the graph based on three physical constraints. The range constraint requires that Euclidean distance between any two connected nodes not exceed the configured maximum link distance. The degree constraint ensures that neither node exceeds the maximum number of laser terminals. The line-of-sight constraint verifies that the candidate link does not intersect the Earth, calculated using vectorized segment–sphere intersection with an 80 km atmospheric buffer.

The graph construction uses a greedy spatial strategy: for each node, neighbors are queried using a k-dimensional tree (cKDTree) and sorted by distance, then the nearest valid neighbors are connected until the degree cap is reached or no valid neighbors remain. The greedy construction represents a plausible, locally implementable neighbor-discovery protocol and functions as a conservative lower bound on connectivity relative to a globally optimized matching.

From a complexity standpoint, the spatial indexing phase using cKDTree operates in approximately $O(N \log N)$ time, with additional per-node neighbor sorting costs that scale with the search neighborhood size.

2.4 Baseline Configuration and Parameter Sweeps

The simulation was anchored by a baseline configuration representing a large-scale LEO constellation deployment. Table 1 presents the baseline simulation parameters.

Table 1 Baseline Simulation Parameters

Parameter Name	Value
Total number of satellites	5,000
Number of orbital planes	71
Orbital altitude	550 km
Orbital inclination	53°
Maximum inter-satellite link distance	1,000 km
Maximum links per satellite	4
Relative phase offset between planes	1
Statistical replicates for confidence intervals	12

One-at-a-time parameter sweeps were conducted by varying each parameter individually while holding others constant at the baseline values. Table 2 presents the parameter sweep ranges.

Table 2 Parameter Sweep Ranges

Parameter	Range	Increment	Number of Values
Orbital altitude	300–1100 km	200 km	5
Maximum inter-satellite link distance	500–3000 km	250 km	11
Maximum links per satellite	2–5	1	4
Total number of satellites	1000–8000	1000	8
Relative phase offset between planes	0–100	10	11
Number of orbital planes	10–130	20	7
Orbital inclination	30°–90°	10°	7

2.5 Graph Metrics

The topological health of the network was evaluated using several graph metrics. The Giant Component Fraction represents the ratio of nodes in the largest connected cluster to the total number of nodes. The Susceptibility, denoted by χ, is the sum of squared sizes of finite clusters excluding the giant component. The Algebraic Connectivity, represented by λ_2, is the second smallest eigenvalue of the graph Laplacian. The Global Clustering Coefficient is the ratio of closed triplets to connected triplets. The Average Path Length is the mean number of hops required to connect any two nodes, calculated via shortest path on a representative sample of node pairs using a sample fraction of 0.7.

Algebraic connectivity is computed with a size-dependent strategy: for networks with fewer than 500 nodes a dense eigendecomposition is used; for larger GCCs an iterative Lanczos method with shift-invert is used to extract the smallest non-zero eigenvalues. The numerical tolerance for iterative solvers is set to 10^{-6}.

2.6 Statistical Analysis & Reproducibility

All attack/robustness curves are averaged across **12 independent replicates**. For each fraction f of satellites removed the sample mean and a two-sided 95% confidence interval computed from the replicate sample using Student's t distribution with degrees of freedom $df = 11$ is reported. Concretely, for a sample mean $\bar{x}$ with sample standard deviation s over n replicates the interval used in the figures is

$$\bar{x} \pm t_{1-\alpha/2,\,n-1}\,\frac{s}{\sqrt{n}}, \qquad \text{with } n = 12,\ t_{0.975,11} \approx 2.201. \tag{2}$$

Correlation values reported in the correlation heatmap are Pearson's r computed across the discrete sweep points for each one-at-a-time parameter. To convert a Pearson r to a two-tailed p-value, the usual transformation to a t statistic is used:

$$t = r\sqrt{\frac{n-2}{1-r^2}}, \qquad p = 2\left(1 - F_{t,\,n-2}(|t|)\right), \tag{3}$$

Here $F_{t,\,\nu}$ denotes the cumulative distribution function of Student's t with $\nu = n - 2$ degrees of freedom and n is the number of sweep samples for that parameter (Table 2 lists the sample sizes). Because sweep sample sizes differ across parameters, reported p-values should always be read alongside the corresponding n.

For reproducibility the experiments used deterministic RNG seeding: path-sampling was initialized with a fixed seed (the integer 42) so that the same node-pair samples can be reproduced; the sequence of replicate seeds was generated deterministically by starting from a fixed integer (nine hundred and ninety-nine) and advancing by a fixed increment for each subsequent replicate, ensuring independent but repeatable replicates; for each replicate and for each fraction value a fraction-dependent integer (the fraction multiplied by 100,000 and rounded to an integer) was added to the replicate seed to obtain the per-fraction RNG.

2.7 Short note on interpretation

Because the correlation analysis uses discrete, finite one-at-a-time sweeps (with sample sizes defined in Table 2), strong Pearson r values (for example $r \approx 0.99$ for maximum degree versus plane resilience) should be interpreted as empirical associations inside the sampled parameter ranges rather than universal causal laws. The greedy adjacency construction and static snapshot methodology are modeling choices that affect numeric thresholds but not the qualitative relationships reported here.

3. Percolation Phase Transition Analysis

The percolation phase transition represents the behavior of network formation in LEO constellations. The simulation results show a consistent pattern across parameter sweep configurations, suggesting that the emergence of global connectivity is governed by geometric principles.

Across parameter configurations, the Walker Delta constellation exhibits a characteristic phase transition pattern. At low satellite densities below 350 satellites, the Giant Component Fraction remains near zero (0.02 at both 50 and 200 satellites), indicating a fragmented network. The first

significant connectivity emerges at 350 satellites with a Giant Component Fraction of 0.26. The critical percolation threshold occurs between 650 and 800 satellites. At 650 satellites, the Giant Component Fraction is 0.23, but by 800 satellites, it jumps to 0.90. Full global connectivity with a Giant Component Fraction of 1.0 is achieved by 1400 satellites across configurations tested.

The susceptibility exhibits peaks at the critical threshold around 800 satellites, coinciding with the steepest rise in Giant Component Fraction. This alignment indicates that the transition point represents the regime of maximum connectivity volatility, where small additions of satellites can cause changes in global network structure.

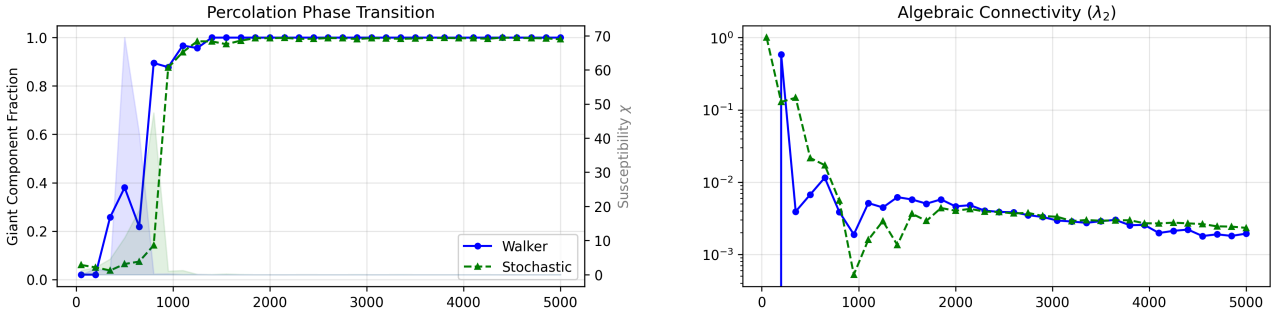

Figure 1 Percolation phase transition showing Giant Component Fraction and Susceptibility (left), and Algebraic Connectivity λ_2 (right) as functions of satellite count. Simulation configuration: 5000 satellites at an inclination of 53° and an altitude of 550 km distributed into 71 planes with an ISL range of 1000 km. Each satellite can connect with up to four others at a time.

The algebraic connectivity transition shows a pattern: it spikes during the percolation transition reaching values close to 10^{0} and 10^{-1} at the earliest connected regimes, then decays as satellite count increases toward 5000, settling near 10^{-3}. The correlation heatmap reveals that satellite count has a negative correlation of −0.81 with the final Fiedler value, indicating an inverse relationship between scale and spectral cohesion.

4. Altitude Analysis

Orbital altitude was swept from 300 km to 1100 km in 200 km increments. The Giant Component Fraction progression is largely invariant across altitudes: the same topological density yields similar percolation thresholds when angular spacing is preserved. The correlation heatmap shows negligible correlation (near 0.00) between altitude and the final Giant Component Fraction, consistent with scale invariance of angularly-regular Walker arrangements.

Altitude influences masking metrics in the sampled range: maximum masking increases with altitude, while area masking shows a negative trend. These observations indicate altitude affects

the severity and temporal extent of masking once the masking zone is exited, even though the percolation threshold itself is topologically stable.

5. Maximum Link Distance Analysis

The maximum inter-satellite link distance was swept from 500 km to 3000 km in 250 km increments. Longer link distances reduce the severity of the masking effect: peak masking and integrated masking area decline as D_max increases. When the maximum link distance is large the network becomes more mesh-like and the distinction between random and targeted plane attacks diminishes. Benefits plateau beyond roughly 1500 km in the sampled regime.

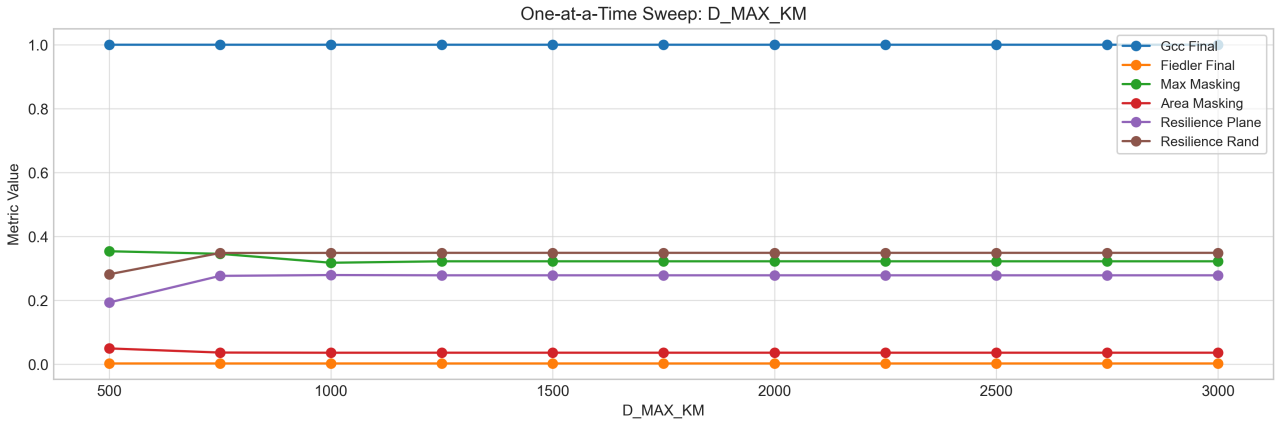

Figure 2 One-at-a-time parameter sweep for maximum link distance (D_MAX_KM). Maximum masking decreases with longer link distance while resilience metrics plateau beyond approximately 1500 km.

6. Maximum Degree Analysis

Maximum degree (allowed links per satellite) was swept from 2 to 5. Maximum degree exhibits the strongest empirical relationship with resilience metrics among parameters tested. Within the sampled range, plane attack resilience correlates very strongly with maximum degree (reported Pearson $r \approx 0.99$) and random failure resilience similarly strongly (reported $r \approx 0.96$). These associations indicate that adding terminals per satellite is an effective lever for improving network survivability in the tested regime.

Masking behavior varies non-monotonically: peak masking is largest at an intermediate degree (degree = 3 in the sampled points) and declines for higher degrees. This indicates that while increasing degree raises absolute resilience, the relative difference between random and targeted attacks can be largest at intermediate degrees.

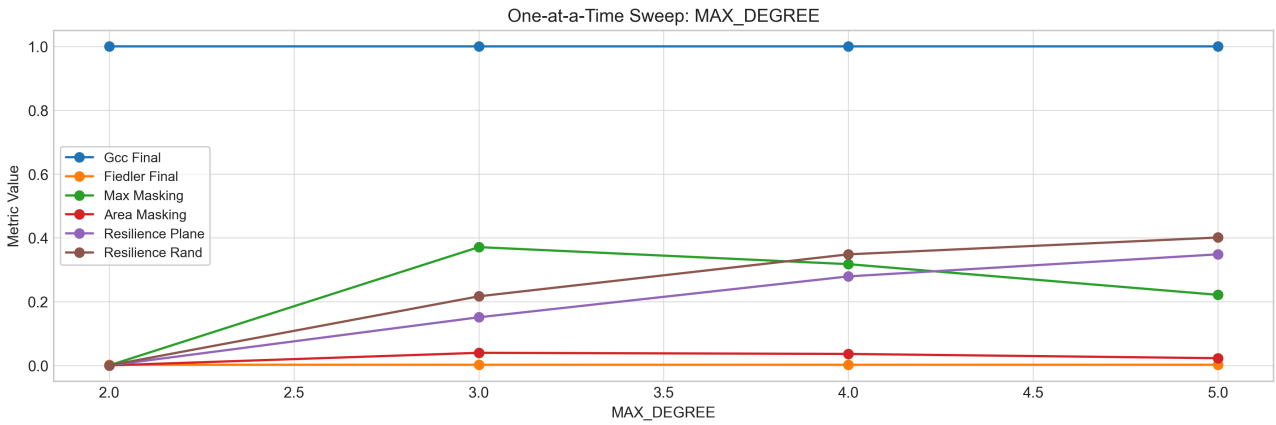

Figure 3 One-at-a-time sweep for maximum degree. Both resilience metrics increase with degree, while peak masking is maximized at intermediate degree values.

The masking threshold in the sampled regime shifts with degree: approximately 15% removed at degree = 2, ~20% at degree = 3, and ~25% at degrees 4–5. This parameter sensitivity suggests small degradations in terminal availability can change the point at which hidden structural vulnerabilities become visible.

7. Constellation Density Analysis

Satellite count was swept from 1000 to 8000 in increments of 1000, with the number of planes scaled as the square root of satellite count. Resilience metrics improve rapidly between 1000 and 3000 satellites and show diminishing returns beyond approximately 4000. Correlation patterns indicate larger constellations yield higher absolute resilience but poorer per-node spectral cohesion (final Fiedler value trends downward with N in the sampled regime).

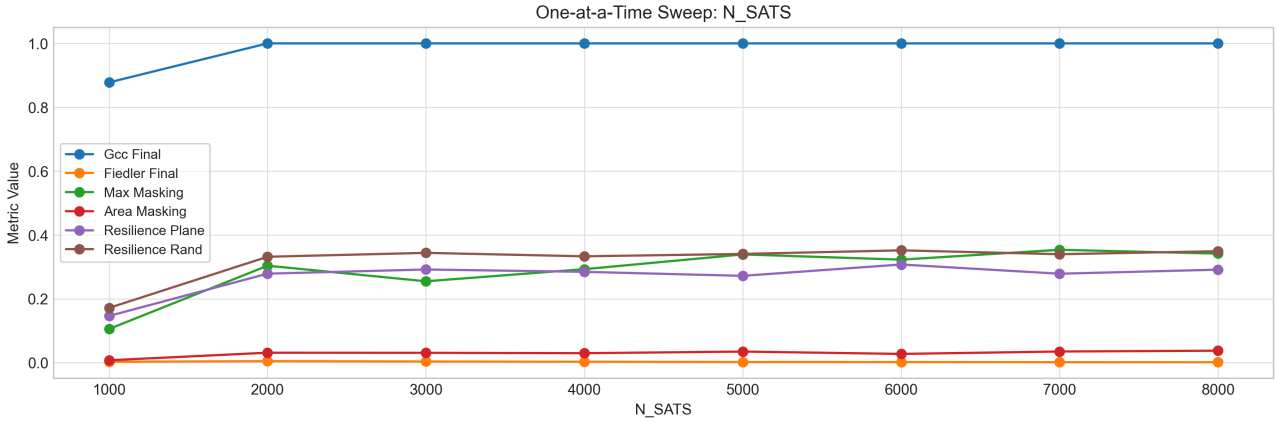

Figure 4 One-at-a-time sweep for satellite count. Resilience metrics improve rapidly from 1000 to 3000 satellites; marginal gains decline beyond 4000 satellites.

8. Phasing Analysis

Phasing was swept from 0 to 100 (unitless phasing parameter) in steps of 10. Most metrics show weak or negligible correlations with phasing in static snapshots; phasing effects are likely more salient in dynamic scenarios where temporal link formation affects routing and handovers, which are outside the scope of this static analysis.

9. Orbital Plane Count Analysis

Plane count was swept from 10 to 130 in steps of 20. Plane count shows a strong negative correlation with plane attack resilience (reported Pearson $r \approx -0.91$), one of the most pronounced relationships in the sweep study. Holding total satellite count fixed, increasing planes dilutes within-plane redundancy and increases vulnerability to the removal of an entire plane.

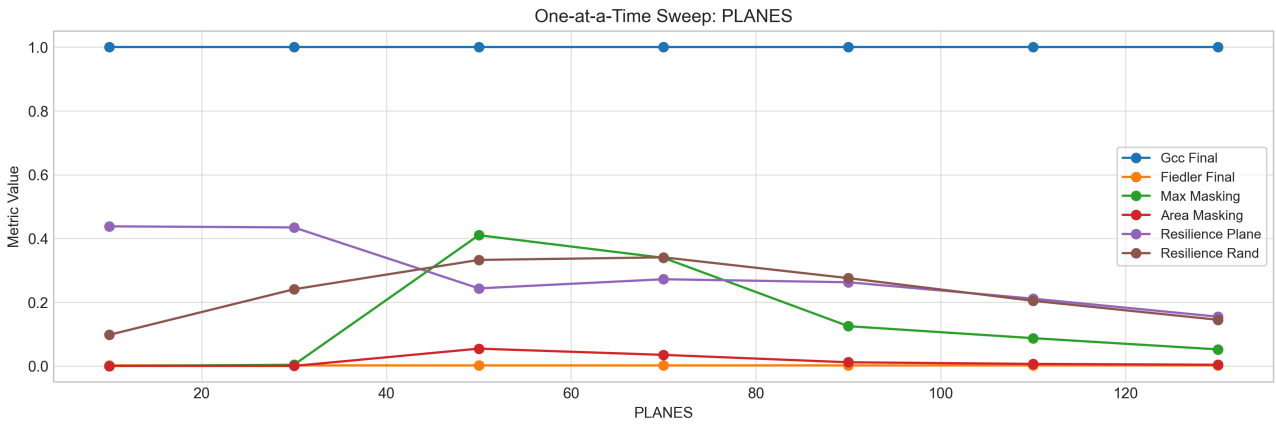

Figure 5 One-at-a-time sweep for orbital plane count showing declining plane attack resilience as plane count increases.

10. Inclination Analysis

Inclination was swept from 30° to 90° in 10° increments. Resilience metrics peak in the 50°–60° range in the sampled points, with degraded performance at very high inclinations due to polar clustering effects that reduce cross-plane bridging links.

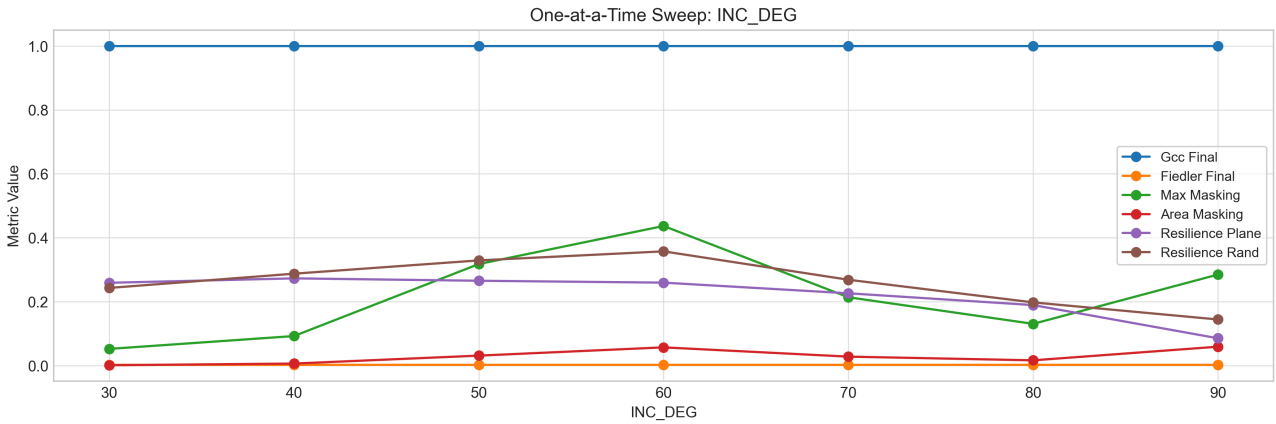

Figure 6 One-at-a-time sweep for inclination. Resilience peaks in the 50°–60° band and declines at higher inclinations.

11. Synthesis and Conclusions

11.1 Key Empirical Findings

Several empirical findings emerge from the parameter sweep analysis. Maximum degree is the dominant robustness lever in the sampled range: strong Pearson correlations with plane and random resilience are observed (e.g., $r \approx 0.99$ and $r \approx 0.96$, respectively). Plane count has a pronounced negative relationship with plane attack resilience ($r \approx -0.91$). Inclination effects are non-monotonic, with the 50°–60° band showing superior resilience in the sampled points. Maximum link distance delivers most of its resilience benefit before approximately 1500 km.

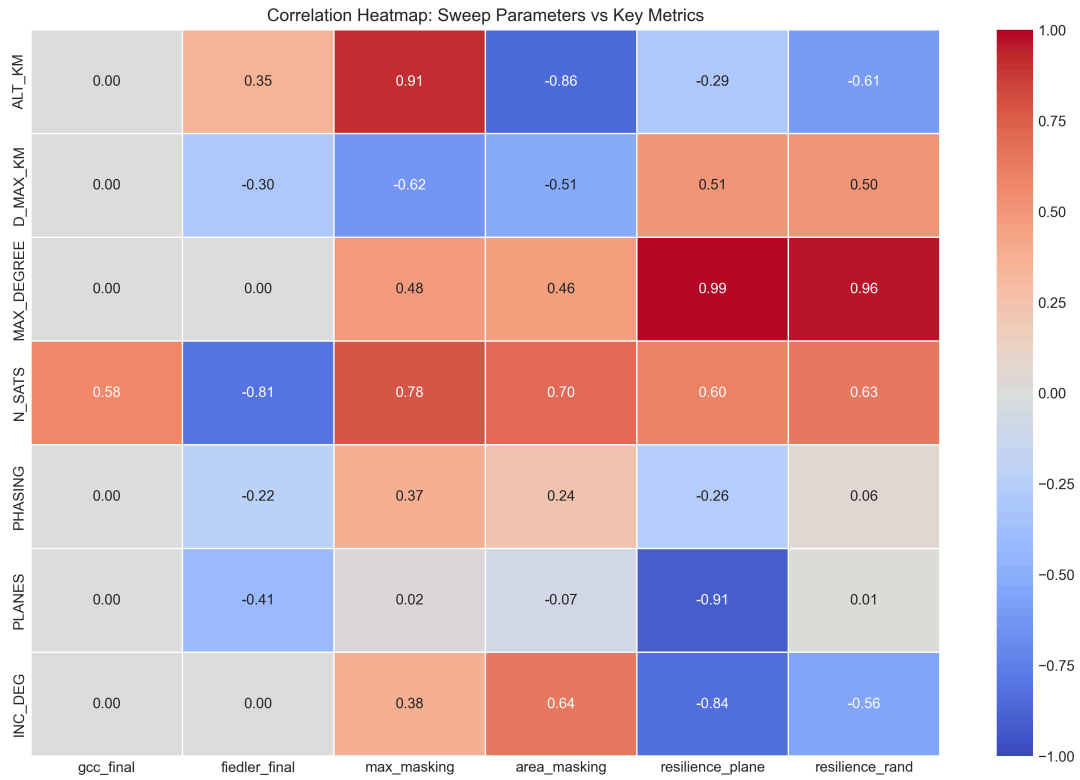

Figure 7 Correlation heatmap showing relationships between sweep parameters and key metrics. Values are Pearson r computed across the discrete sweep samples (see §2.6 for sample sizes and p-value conversion guidance). Notable strong associations include maximum degree with resilience metrics and plane count with plane resilience.

11.2 Recommendations

Practical recommendations derived from the empirical sweeps: provision for more inter-satellite terminals per satellite (higher maximum degree) materially improves survivability; prefer fewer planes with more satellites per plane when attack resilience is a priority (subject to coverage trade-offs); select inclinations in the mid-latitude band (50°–60°) when resilience and coverage are jointly important; and design ISL hardware to support ranges in the 1000–1500 km band to capture most robustness gains without excessive engineering cost. The masking threshold observed (roughly 15–25% removed depending on configuration) suggests an operationally meaningful region where redundancy can conceal structural vulnerabilities. Operators and designers should monitor intermediate removal fractions closely and consider cross-plane and inter-shell redundancy mechanisms as mitigations. Note that this region is almost exclusively dependent on the maximum links per satellite -- results show that generally, four linkages per satellite results in a deceptively redundant region up until the 20% removal mark.

11.3 Limitations and Future Work

Limitations include the static snapshot methodology (no dynamic handover modeling), one-at-a-time sweeps that do not reveal parameter interactions, and simplified propagation/occultation modeling (Earth + 80 km buffer, no atmospheric refraction). Future work should include targeted interaction sweeps, dynamic simulations across orbital phases, and examination of multi-shell architectures.

References

Callaway, D. S., Newman, M. E. J., Strogatz, S. H., & Watts, D. J. (2000). Network robustness and fragility: Percolation on random graphs. *Physical Review Letters*, 85(25), 5468–5471.

Cohen, R., Erez, K., ben-Avraham, D., & Havlin, S. (2000). Resilience of the Internet to random breakdowns. *Physical Review Letters*, 85(21), 4626–4628.

Fiedler, M. (1973). Algebraic connectivity of graphs. *Czechoslovak Mathematical Journal*, 23(98), 298–305.

Handley, M. (2018). Delay is not an option: Low latency routing in space. *ACM HotNets*.

Portillo, I. D., Cameron, B. G., & Crawley, E. F. (2019). A technical comparison of three low earth orbit satellite constellation systems to provide global broadband. *Acta Astronautica*, 159, 123–135.

Kassing, S., & Wichtlhuber, M. (2022). OneWeb and Starlink: A comparative analysis of LEO mega-constellations. *Computer Communications*, 191, 179–191.

Giambene, G., & Kota, S. (2021). Satellite constellation design for real-time applications. *IEEE Communications Magazine*, 59(9), 44–49.

Rao, Y., Zhang, Y., & Zhang, L. (2023). Temporal graph analysis of LEO satellite networks: Connectivity and routing. *IEEE Transactions on Aerospace and Electronic Systems*, 59(4), 4567–4580.

SpaceX. (2024). Starlink satellite network specifications and orbital parameters. *FCC Filings*, SAT-MOD-20240115-00012.

Amazon. (2023). Project Kuiper constellation design and deployment plan. *FCC Filings*, SAT-LOA-20230720-00115.

Chen, Q., Giambene, G., & Yang, L. (2022). Analysis of inter-satellite link paths for LEO satellite networks. *IEEE Access*, 10, 44512–44524.

Strogatz, S. H. (2001). Exploring complex networks. *Nature*, 410(6825), 268–276.

Walker, J. G. (1984). Satellite constellations. *Journal of the British Interplanetary Society*, 37, 559–571.